DATA PROCESSING FOR LASER BEAM IMPACT MODELLING

Jana HÁJKOVÁ

Department of Computer Science and Engineering
University of West Bohemia
Univerzitní 8
306 14 Pilsen, Czech Republic
e-mail: `hajkovaj@kiv.zcu.cz`

Communicated by Michael M. Richter

Abstract. This paper sumarizes the data preprocessing methods used for modelling of laser beam impact. At the beginning, it gives a short overview of physical background of interaction between a laser beam and processed material. Also the input data sets are described and the way of their acquisition is shown, so that the reader could get a good idea of the whole problem. The main content of the paper is formed by description of the data preparation process that consists of several steps – automatic heat-affected area detection, samples parameterization and their surface approximation. In all cases our methods with the best results are described in a detail. At the end of the paper, our results are summarized, discussed and possible plans for the future research are introduced.

Keywords: Laser engraving, simulation, modelling, height map, detection, parameterization, approximation, material surface

1 INTRODUCTION

The work described in this paper is a part of a larger project that deals with laser engraving control and modelling of laser engraving process. We are interested in the processing of the measured data, its visualization and laser engraving modelling and simulation. For our work, we use data of real samples engraved by a laser and measured by a confocal microscope. Basics of data acquisition and its format are outlined in Section 1.2.

The main part of the paper describes preprocessing of real data. Samples are parameterized and from the set of computed parameters a new sample surface can be artificially generated. Our solution of these problems is described in Sections 2.2 and 2.3. Several times during the data preprocessing we need to detect the area modified during the engraving process by the laser beam (e.g. for the sample parameterization or comparison of samples). Our approach is explained in Section 2.1. To understand the real data well, we had to analyze the real engraved samples. Therefore we learned about the structure of the sample as much as possible in order to understand the physical background of the laser engraving process (for details, see Section 1.1). Finally, data preprocessing results are summarized in Section 3. Section 4 concludes the paper.

1.1 Laser-Engraving Process

To be able to model samples engraved by laser beam, we have to understand the process of laser engraving well. Laser beam is an electromagnetic radiation. When this radiation strikes a surface of the material, some radiation is reflected, some absorbed and some transmitted. For laser processing of a material, the most important is absorption of the radiation which causes excitation of free electrons (in metals), vibrating in the material structure (in insulators), or both (in semiconductors). We detect all these processes as heat. The heat generated at the surface that is directly affected by the laser beam is conducted into the material. If the laser intensity is high enough, the incident material heats, melts and if it reaches the boiling point, it starts to vaporize. The three phases can be seen from the cross-section view in Figure 1. The solid arrows indicate the laser beam direction, dashed arrows show the heat conduction in the material and the molten and vaporized material is highlighted with gray color.
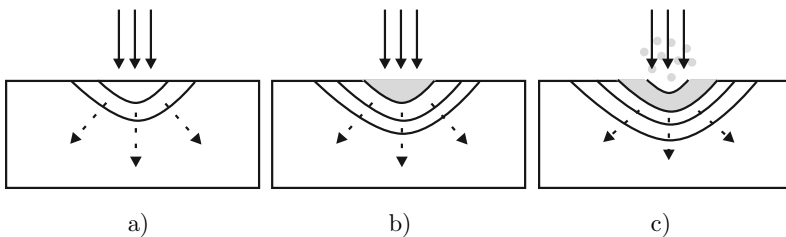

Fig. 1. Laser–material interaction phases: a) heating, b) melting, c) vaporization

Once vaporization has been initiated, vapor interacts with the laser, and ionizes. Highly ionized vapor is called plasma. Vaporized particles, which are not affected by the laser beam, move away from the surface of the material, lose their energy and approximately 18 % of them condense back to the surface [3]. Moreover, vapor evolving from the surface exerts a recoil pressure on the surface, which causes melt

expulsion, schematically shown in Figure 2. The whole process and the details related to the plasma phase are also described in [2, 4, 5, 18].
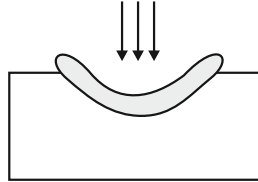

Fig. 2. Schematic representation of melt expulsion process

Finally, at the exposure site, a pit with a transition ring around it is left behind (as shown in Figure 3).
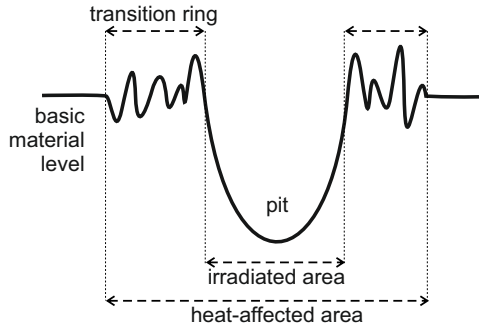

Fig. 3. Relief of a sample and the used terminology

1.2 Data Description and Aquisition

To obtain the data for simulation input, real samples have to be engraved by an existing laser equipment into a real material and then measured. For each combination of a laser device configuration and a material, which is used for the simulation, a special data set has to be prepared. Such set of data is called experiment. It consists of samples engraved by the laser into a single point in the material. The number of pulses goes in sequence, e.g. from 1 to 100 (in Figure 4, each pulse from the sequence is engraved in a separate row).

After re-burning the same pulse several times while keeping the same conditions, the results differ a little. Hence, each pulse count is repeated several times in order to get an average result. Samples engraved by the same number of laser beam pulses under the same conditions and laser settings are called 'similar samples' in the following explanation. All samples we use are engraved by laser device BLS-100 (Nd:YAG solid-material, lamp-pumped laser with wavelength of 1 064 nm) into
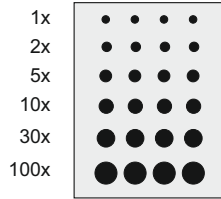
Fig. 4. The experiment layout

steel and cermet (a composite material composed of ceramic and metallic materials). Parameters of burning are as follows: laser power 100 W, current 28 A, ray width 0.01 mm, diaphragm 1.8.

After the samples are engraved, they have to be measured. For this purpose, confocal microscope Olympus LEXT OLS3100 is used. During the measurement we focus only on one part of the material containing the engraved pulses. Resolution and zoom are chosen, the material sample is scanned by confocal microscope and the measured data set is saved into a file.

The description of each measured real sample is stored in the format of a height map. This height map is formed by a matrix of real numbers, which express the heights in a uniform rectangular grid.

To get a better idea about the appearance of a real sample see Figure 5, where the 3D view on the sample and its cross-section are shown. The cross-section relief contains several typical features, which have resulted from the engraving process described in Section 1.1 and the character of used material. As can be seen, the heat-affected area is not so well-bordered in comparison with the simplified relief shown in Figure 3. The not-well-bordered heat-affected area causes the main problem that is to be solved in automatic detection methods.
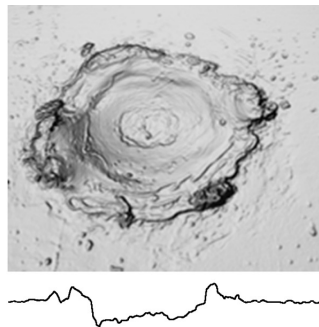

Fig. 5. 3D view on a sample with 100 laser pulses engraved into steel and its cross-section

Because during data preprocessing we also need to parametrize and approximate the surface of the sample, we have to explore the sample surface in more detail.

The real samples are measured in a very high level of detail and during careful exploration, we can find the bumps originating from irregularity in the material surface. In addition to material roughness, local defects in the material can be detected here and there. Their size is variable and they are placed on the sample surface completely randomly (Figure 5). The size of the irregularities depends on the used material. The central part of the pulse (i.e., the area irradiated directly by the laser beam) is also smooth and the bottom of the pit is a little bit rougher (Figure 6 a)). The most ragged surface part is the transition ring. The surface is modulated by some concentric waves that are both regular (Figure 6 b)) and irregular (Figure 6 c)). Sometimes local defects with a considerable roughness can appear, especially at the outer border of the transition ring (Figure 6 d)). They are caused by the ablated material that becomes cool and deposits in the area next to the pit irregularly. At the outer border, roughness declines slowly and fades into roughness of the bulk material.

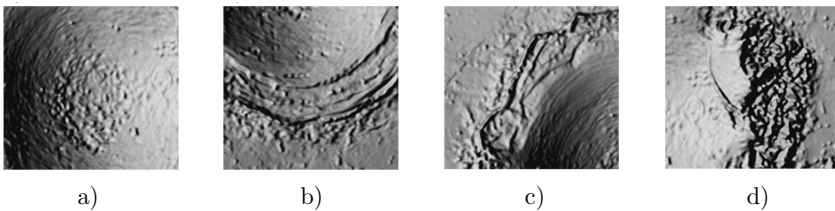
a)   b)   c)   d)

Fig. 6. Examples from different parts of a typical sample surface

If we engrave the same sample for a second time, the result will never be the same because at least the surface of the base material differs. Nevertheless, samples burned into the same material are similar. Some characteristics of the burned sample depend directly on the used material itself, some of them depend on the number of laser pulses engraved into the material surface. That is why, for the modelling of the sample surface, we can use parameterization to get a set of sample descriptors and approximation to generate the material surface artificially. Our approaches are described in the following sections.

2 DATA PREPROCESSING

Data preprocessing runs in several steps. When we get a sample, the heat-affected area has to be detected first, so that we know, which part of the sample should be further processed. In the next step, parameterization of the heat-affected area is provided. From the set of computed parameters any artificial sample surface can be generated as an approximation of the original one. Our methods designed to solve these particular problems are explained in the following sections.

2.1 Heat-Affected Area Detection – Statistical Method

The main task of the heat-affected area detection is to define the area of the material surface affected by the laser beam during the burning process as exactly as possible. The detection should be used several times during the process of the laser-burned samples simulation, e.g. during parameterization of the sample or if we want to compare two samples.

The main problem during the process of pulse detection is the basic material surface roughness. As can be seen in Figure 7, the surface of some materials is quite smooth (such as the surface of steel in Figure 7 a)) but in some cases material surface roughness is more noticeable, like in the case of cermet (Figure 7 b)). Moreover, on the surface of some materials local defects can appear as well. Such defects do not need to be visible on the material surface by naked eye, but due to the high resolution of the real sample scanning, they are included in the description of the sample and they are a source of problems during automatic pulse detection.
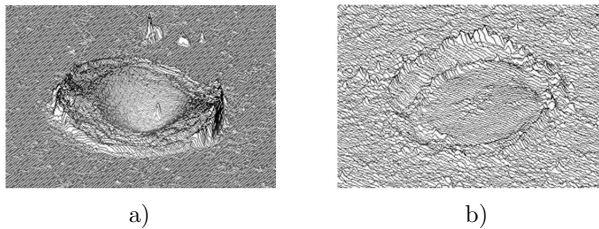

a)   b)

Fig. 7. a) Steel with relatively smooth surface; b) cermet sample with globally higher surface roughness

The user is able to distinguish material roughness and pulse border well, but for an automatic method it is difficult to differentiate them. If we want to use the pulse detection as a part of the whole data preprocessing, we cannot build on manual data processing; but still precision and accuracy of detection has to be preserved during the process automation.

We have designed several methods using various computing approaches to find the most reliable method for detection of the heat affected area in any sample. Some of them are also described in [6]. Their efficiency depends especially on the processed sample material. Because the detection method should be used as a part of the authomatic data preprocessing, it has to detect the pulse effectively independently from the used material. In the following description, our method with the best results (the statistical method) is explained.

The basic idea of the statistical method comes from computation of sample surface statistical qualities and from utilization of this knowledge for the pulse area recognition.

First, the whole sample height map is divided into regular rectangular grid and for each cell of the grid a representing value is computed. By this operation, we get

simplification of the height map representation that can be further processed. It is very important to determine the proper size of the statistical grid cell to simplify the sample enough, but not too much. For each cell the representing value has to be computed. We need to differentiate the heat-affected area from the base material. The best results are given with computation of the difference of minimal and maximal height in the statistical grid cell. To eliminate surface irregularities, the values are truncated to integers. An example of the array of representing values for a concrete sample can be seen in Figure 8 a). We can see there clearly that for the heat affected area of the pulse the computed values in the grid are not zero, while the base material level of the sample is represented by zeroes. Non-zero values also appear in places with a large local defect (an example can be found in the top right part of the sample) in Figure 8 a).

Now, to detect the pulse area, we have to decide which values of the statistical grid should be included as heat-affected-area-representing and which should not. If a grid cell that represents values for heat-affected area and base material can be distinguished well, we can use for example thresholding to separate them. In our case all values lower than 1 were thresholded as background and values greater than or equal to 1 were determined as objects. A new mask is created for the whole sample – all values of the background are masked as zero (non-pulse) and the cells representing objects are indicated by the value of 1 in the mask. Our testing sample and its thresholded mask are shown in Figure 8 b). Cells marked as pulse (with the value of 1 in the mask) are highlighted with the lighter color, non-pulse cells are drawn with dark gray.
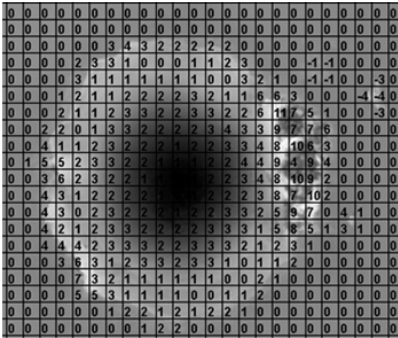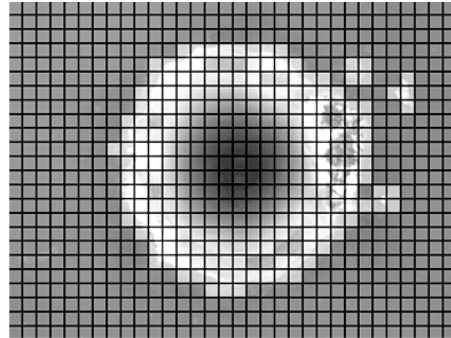
a)   b)

Fig. 8. Sample engraved into steel; a) for each grid cell, its representing value is computed; b) sample with the highlighted mask computed above the statistical grid

Sometimes, as shown in the example in the right top corner, not only the area of the pulse is highlighted. If there is any larger local defect on the material surface, the value of the computed difference in the corresponding grid cell is higher than the threshold for a base material and so the cell can be thresholded as an area of

the pulse. Because we want to detect the heat affected area as exactly as possible, we have to remove local defects and other irregularities. We can suppose that the heat affected area is the largest continual area marked in the mask with the value of 1. Therefore, we should be able to provide segmentation of the result.

Image segmentation is the process of partitioning a digital image into multiple segments (sets of pixels) [1, 17]. The best fitting algorithm for our purpose seems to be the algorithm of binary image segmentation described e.g. in [10, 16], namely the connected component labeling method. We decided to use a modified row-by-row labeling algorithm.

During this process, each separate segment of the image (in our case each separate object in the mask) is labeled with a consecutive natural number. This segmentation algorithm is a sequential process. We have to go through the image (mask after thresholding) row by row and process each single pixel (cell of the mask) that is marked as an object (in our case the value of the processed mask cell has to have the value of 1). The other pixels (cells) are ignored because they are part of the background. The algorithm makes two passes over the mask.

In the first one, each cell representing the object area is labeled with a positive integer according to its neighbors. The whole process is explained on the example of a small grid shown in Figure 9, for each step the processed cell is bolded, and the equivalence table is shown. The grid is processed row by row and each single cell is labeled according to three simple rules:

1. If no labeled cell is found in the neighborhood of the processed cell, it is labeled as a new segment (Figure 9 a), c), e), g)).

2. If any or all cells neighboring with the processed cell are labeled with the same number, the processed cell is also labeled with the same integer (Figure 9 b), d)).

3. However, if more neighboring cells are labeled with different numbers, the processed cell is labeled with the biggest of them and collision has to be registered (Figure 9 f), h), i)) into the equivalence table.

During the second pass, objects are relabeled according to the equivalence table so that the same number is used to represent objects with colliding numbers. As a new labeling number the maximum from the equivalence table is used. The relabeled cells are bolded again (see Figure 9 j)).

At the end, several objects separated with different labels can be found on the surface (Figure 8 b)). To get the right one (the heat-affected area) we get the largest labeled area (the area with the highest number of the mask cells) that is declared as a heat affected area. The other objects detected by the segmentation are ignored and for the only segment remaining in the mask the bordering rectangle is computed. Results of the automatic pulse detection by the proposed statistical method can be found in Section 3.1.
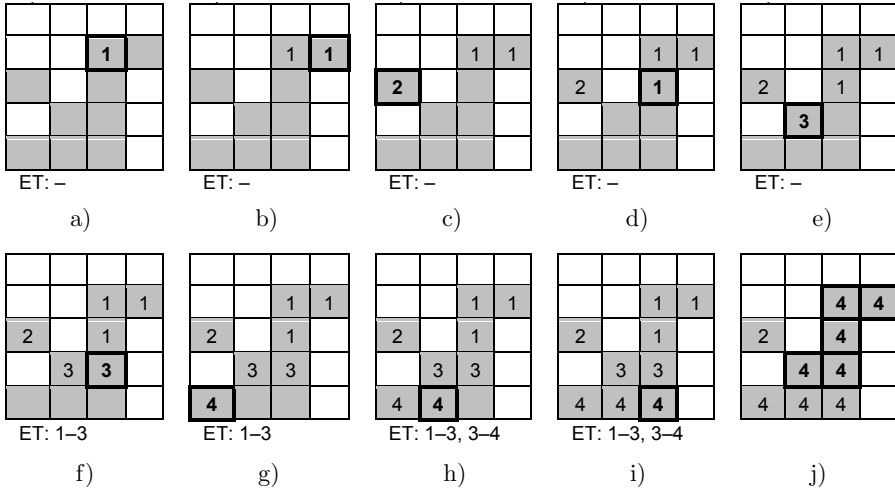
Fig. 9. Modified row-by-row labeling algorithm: a)–i) the first pass (an object is labeled with several numbers); j) objects are relabeled according to the equivalence table

2.2 Sample Parameterization

To get information about the pulse shape, we use cross-sections throught the sample surface. Because heat-affected areas are not symmetric, we cannot use cross-sections measured only in one direction. Our experiments show that two orthogonal cross-sections going through the center of the pit are sufficient. Because of the character of heat-affected areas in most cases the cross-sections are orthogonal and correspond to cross-section parallel to x and y axis.

Samples are most similar in the area of the pit. As mentioned in Section 1.2, surface of the pit is quite smooth and slight roughness is perceptible in the bottom part. On the contrary, the border of the transition ring, formed by the melten material, is different for each explored case.

We can distinguish two groups of parameters. The first one includes parameters describing the basic shape of the sample (such as pit depth, dimension of the inner and outer border of the transition ring or maximal ring height). All these values can be computed from the extracted cross-section for each sample separately without any essential problems (as shown in Figure 10).

The other group of parameters serves for description of roughness and irregularities of the sample. Parameters are often similar to samples engraved into the same material, but so far they are determined experimentally and automation of their computation is part of our future plans.
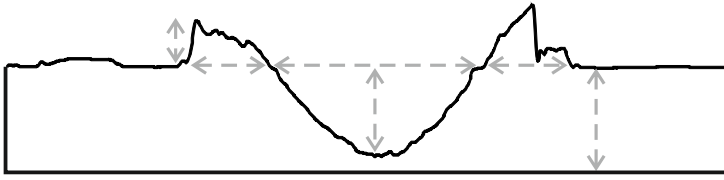
Fig. 10. Computation of parameters describing the basic shape of the sample

2.3 Sample Surface Approximation

As mentioned in the previous sections, the approximation has to be done in two phases. First, we have to determine the basic shape of the approximated sample and then to modify the smooth surface by generating its roughnesses and irregularities. The whole process of the artificial sample surface generation is outlined in the following explanation. The whole methods are described in the cited papers.

The basic shape of the approximated sample was mathematically derived according to approaches found in [15, 19]. Because both parts of the heat-affected area (i.e. the pit and the transition ring) differ a lot, we decided to approximate them separately by two different functions and especially to differentiate the way of surface roughness description. Both generated surfaces are finally connected into the final shape. The whole derivation of the equations can be found in [8].

Both parts were derived in 2D from the cross-sections first. The basic shape of the pit cross-section corresponds with the shape of the plot of a quadratic function. As an example the cross-sections of three similar samples with 100 laser pulses engraved into steel and their approximation are shown in Figure 11.

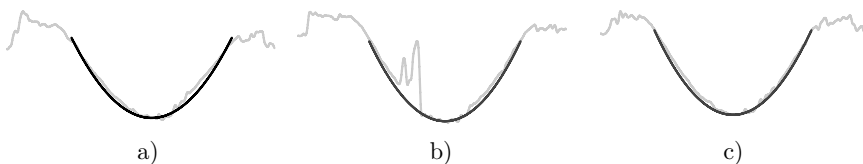a)   b)   c)

Fig. 11. Cross-sections of similar samples and their approximation by parabola

If the pulse pit can be approximated by parabola in each of its cross-sections, the whole pit can be approximated by an elliptical paraboloid. Because we need the paraboloid going through the top border of the pit, the equation representing it has to be modified as follows:

$$z = pitDepth - \left(\frac{(x - x_0)^2}{a^2} + \frac{(y - y_0)^2}{b^2} \right) + z_0. \tag{1}$$

The origin of the solid lies in $S[x0, y0, z0]$, *pitDepth* represents the paraboloid depth and a, b are axes of the ellipse. We need to compute the z value for each point $[x, y, z]$ of the sample surface. The elliptical paraboloid and labeling of its parameters are depicted in Figure 12.
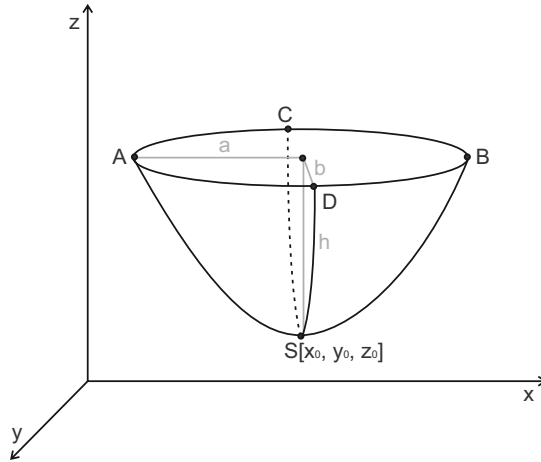

Fig. 12. Elliptical paraboloid and its parameters

Approximation of the area of the transition ring is much more complicated, because the ring shape is irregular and rough. In order to find the approximating function, we had to simplify it first. Also in this case we decided to use parabola for the approximation of the ring cross-section. To do that we need just several parameters, such as base material surface level (*materialLevel*), half of the ring width (*ringRadius*) and maximal ring height (*ringHeight*). Some of them are shown in Figure 13 a).

The whole ring should be approximated by a 3D function. The best solution seems to be the top half of torus which has to be modified for our purposes. Because the ring has an elliptical shape from the top view and the shape of a parabola from the cross-section, the solid representing the ring should be created as the surface of revolution generated by revolving a parabola along the elliptic trajectory in three-dimensional space. Approximation of the whole ring can be done by half of the parabolic elliptic torus which is shown from the top view in Figure 13 b).

To get the proper shape of the resulting torus, we have to recompute the surface according to dimension and elliptical shape of the transition ring, its height and base material level. To get the right result, Equation (2) was derived. To make the equation more simple to read, some of its parts are computed separately in Equations (3) and (4).

a)   b)
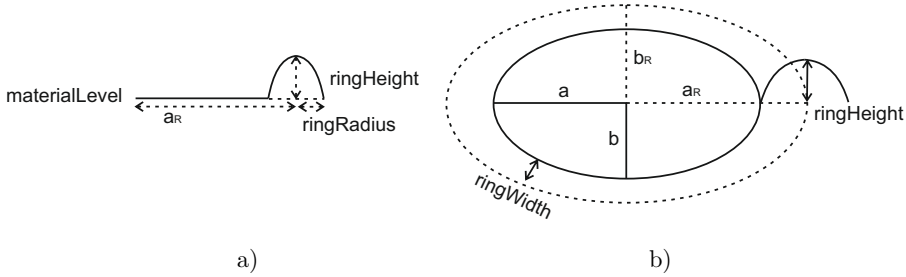
Fig. 13. a) Important parameters for the ring cross-section description; b) description of
      the parabolic elliptic torus from the top view

$$z = -\frac{ringHeight}{\left(\frac{ringRadius}{d_T}\right)^2} * (p-1)^2 + ringHeight + materialLevel \qquad (2)$$

$$p = \frac{(x-x_0)^2}{a_R} + \frac{(y-y_0)^2}{b_R} \qquad (3)$$

$$d_T = \frac{\sqrt{(x-x_0)^2 + (y-y_0)^2}}{p} \qquad (4)$$

Results of the first step of the sample surface approximation can be found in
form of 3D views and cross-sections for several samples in Section 3.2.

Mathematically generated sample is too smooth in comparison to the real one.
That is why it is necessary to modify a generated surface by some kind of artificial
defects that would represent granularity of the material and roughness of various
parts of a real sample. We have to add several different kinds of irregularities (as
mentioned in Section 1.2 and shown in Figure 6). If we engrave the same sample
twice into different places, it will never be the same, because at least the surface of
the base material differs (similar samples were already mentioned in Section 1.2).
That is why we have to enhance the sample generation with random features such
as noise or various defects to get more realistic results.

In our solution, the method with the broadest usage is the Perlin noise func-
tion [12, 13, 14]. Perlin noise combines a noise function with an interpolation func-
tion. 1D Perlin noise is formed by randomly generated values, the distance of which
is given by some frequency. This frequency is defined as 1/wavelength, where the
wavelength represents the distance from one generated value to the next one. The
generated values are interpolated using the Hermit interpolation [20] to get a smooth
interpolating curve with given amplitude (i.e., the difference between the minimal
and maximal generated value) and frequency. If we sum up several curves with va-
rious frequencies and amplitudes, we get the final Perlin noise function. Of course,
we can use the Perlin noise function also in 2D and as a result we get a surface.

The selection of frequencies and amplitudes affects the result. Very often, we work with so called octaves, where the frequency is defined as in Equation (5) and so the frequency of each function is twice as the frequency of the previous one.

$$frequency = 2^i \tag{5}$$

To get the final Perlin noise surface, we can sum up the octaves, whereas each octave is summed up with some amplitude. If the amplitude is high, the octave influences the result more and vice versa. Amplidutes can change depending on the order of octaves (if we use so called persistence), or we can define amplitude vector, where we define amplitudes for each octave separatelly. Exactly this approach works very well in the modulation of sample surface irregularities. Some examples can be seen in Figure 14.
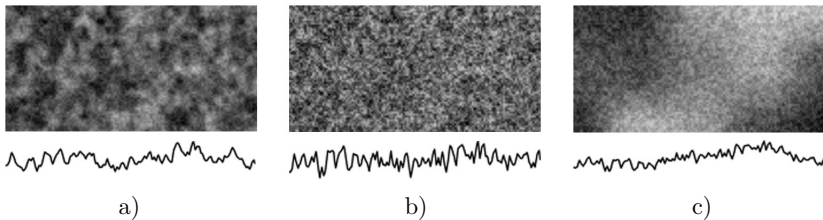

a) b) c)

Fig. 14. 2D Perlin noises generated according to amplitude vectors:
a) $[0.25, 0.25, 1, 1, 0.5, 0.5]$; b) $[0.5, 0.5, 1, 1, 3, 3]$; c) $[2, 0, 0, 0, 0.5, 0.5]$

The variability of the Perlin noise function is high, so we can use it for generating surface roughness to get realistically appearing samples. Perlin noise can be used several times during the pulse generation process. The result depends on the parameters that we used.

The first problem that the Perlin noise can be used to solve is the generation of the pit bottom roughness. Another area where the usage of the Perlin noise is appropriate is the generation of local defects on the transition ring (see Figure 15). To get a better idea of how the generated surface looks compared to the real one. 3D view on local defects in two real samples is shown in Figures 15 a), b). The surface generated by the Perlin noise can be seen in Figure 15 c).

For final modulation we use combination of various masks. At the beginning, we generate a mask of the transition ring (see Figure 16 a)). The area of the ring is represented by the value of 1, the borders of the ring are a linear interpolation between the values of 0 and 1. Then we generate another mask representing the distribution of local defect in the transifion ring area. We can use the Perlin noise for this purpose as well, of course, with other parameters. The second mask is thresholded again, often more threshes are used to get smoother transitions (see Figure 16 b)). If we make an intersection of both masks, we get the result mask shown in Figure 16 c) which serves for the modulation of the Perlin noise described above (Figure 16 d)).
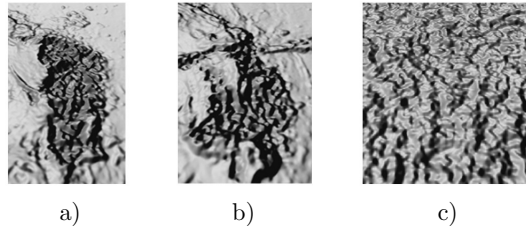
a)   b)   c)

Fig. 15. a)–b) Local defects in two different samples; c) surface generated by the Perlin noise

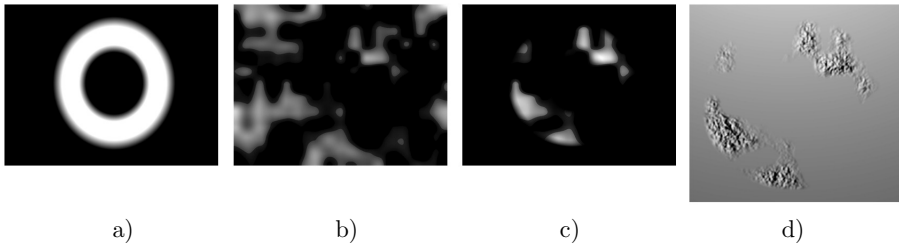a)   b)   c)   d)

Fig. 16. a) Mask of the transition ring; b) mask of the local defect areas; c) intersection of both previous masks; d) final result after the generation of local defects

Except for the sample roughness and local defects in the real samples, concentric waves are also visible in the transition ring area (as shown in Figure 6 b)). These waves are especially noticeable on the outer border of the ring; they are relatively thin and sometimes discontinuous. Their shape consists of a number of edges which form an elliptical shape approximately. If we want to generate waves, we need to know several parameters for their description, such as the dimension of waves, their segmentation, height and width and of course their number. If we know values of these parameters, we can generate waves in the surroundings of the transition ring outer border. Two examples of generated waves modulated on the smooth surface of sample basic shape can be seen in Figure 17.
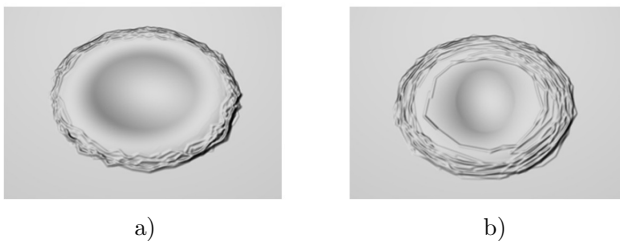

a)   b)

Fig. 17. Examples of a) 20 and b) 30 waves modulated on the smooth sample surface

3 RESULTS

For our tests, we received various real measured samples engraved into steel and cermet from our colleagues who work on the physical part of the project. After their anaysis we received complete measured experiment engraved into steel with the laser mentioned in Section 1.2. To test our methods well samples engraved into both materials with a sequences of laser beam pulses engraved into one point and also with different various zoom choice were used.

3.1 Heat-Affected Area Detection

To present results of the statistical method used for heat-affected area detection, we chose a set of testing samples. We labeled them with capitals from A to H. Some of them are engraved into cermet (A–D), where high roughness of the material influences the detection process and the others are engraved into steel (F–H) which has much smoother surface. Samples with various numbers of laser pulses engraved into a single point of the material were chosen. We have included samples with 1, 2, 70 and 100 laser pulses engraved into cermet and samples with 1, 10, 50 and 100 laser pulses engraved into steel into the testing set. All samples except the first one were measured with the same scale. Surfaces of several samples contain some local defects on the material and shapes of pulses are in some cases more and in some less asymmetric. An areal local defect can be recognized in the surface of the sample in E. It influences both the surface of the heat-affected area and its surroundings. Another local defect affecting the area of pulse that should be detected can be found in H. These types of local defects together with roughness of the sample surface affect the detection most. In sample F, another type of local defect is shown. This defect does not influence the results of the detection algorithms.

To sumarize the results of the statistical method, we can have a look at Figure 18. We prepared several tests for experimental detection of the optimal cell size. For sample A the size of the cell had to be decreased to detect changes on the relatively small area of the pulse. The other samples were measured with the same resolution, and so the optimal size differs only in dependence on the used material. Our tests show that for rougher material, such as cermet (Figures 18 b)–d)), the grid cell size has to be smaller than for the smoother material, such as steel (Figures 18 e)–h)). For all testing samples engraved with the same precision into the same material (B–D and E–H), the same grid size was used.

As can be seen in Figure 18, all testing samples were detected correctly with the statistical method. Grid cell determination size remains the main problem. As shown on our testing samples, the size can be experimentally precomputed, which should be done according to the most problematic samples. The size of a grid for our testing samples has corresponded approximately to 5 % of the heat-affected area dimension.
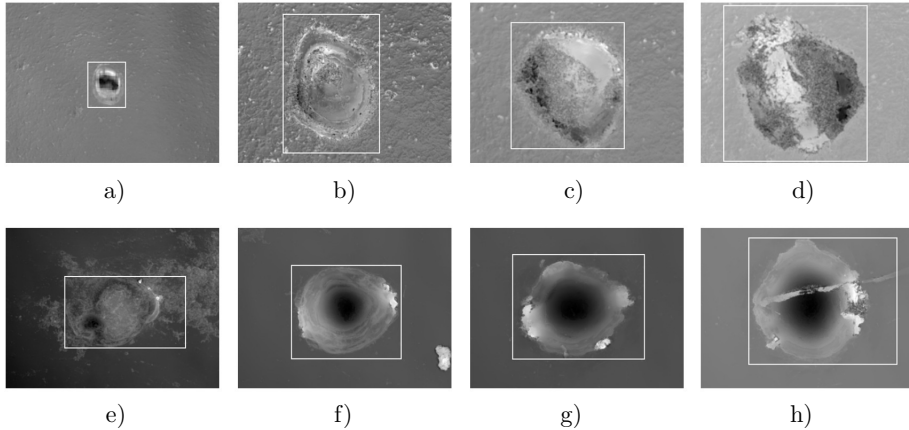
a)   b)   c)   d)

e)   f)   g)   h)

Fig. 18. Results of the statistical method used for automatic detection for samples A–H

3.2 Sample Surface Approximation

The pulse approximation was also tested on various samples. Results for the area of the pit are very successful. More problematic is the area of the transition ring, where the sample surface roughness is high. For the comparison of the original samples with the generated approximations, we used mainly the methods described in [7]. For the following presentation of results, we chose visual comparison.

To obtain the final sample, we have to put all the generated parts together. For the base material, the surface of the measured real sample is used. Then, the basic shape of the pit is computed and its bottom is modified by the Perlin noise. After that, we can generate the transition ring. Its basic shape is computed, the masks for the ring and the Perlin noise are created and then together with waves modulation is used for its modification. Results can be seen from different points of view in the following figures.

First, we compare the original sample with its approximation after the first step (the smooth sample surface) in 2D in the form of two orthogonal cross-sections of both compared samples. Black curves represent cross-sections of the real sample, gray curves show the smooth generated sample surface. Cross-sections in the horizontal direction are shown in Figures 19 a)–c); vertical cross-sections can be seen in Figures 19 d)–f). The first cross-section from each triplet represents the middle of the pulse in the given direction, the others move more to the margin of the pulse.

To compare the complete approximation of the same sample as in Figure 19, we will also start with the 2D view. We compare the original and the newly generated sample in their cross-sections. Black curves represent cross-sections of the real sample and gray curves show the generated sample surface. Cross-sections in the horizontal direction are shown in Figures 20 a)–c); vertical cross-sections can be
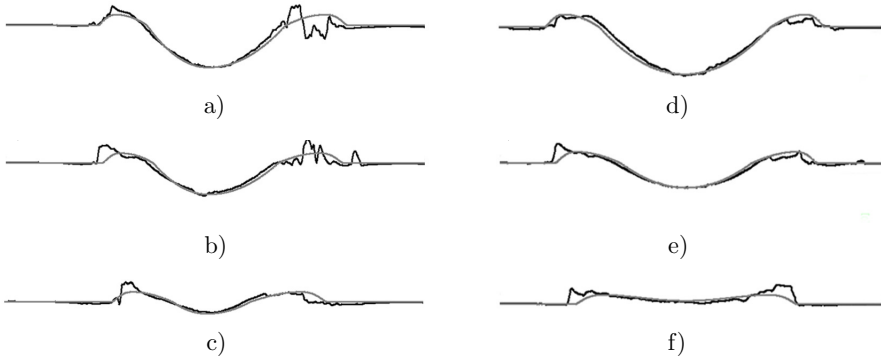
a)

d)

b)

e)

c)

f)

Fig. 19. Approximation of sample with 100 laser pulses engraved into steel by the smooth surface in 2D view
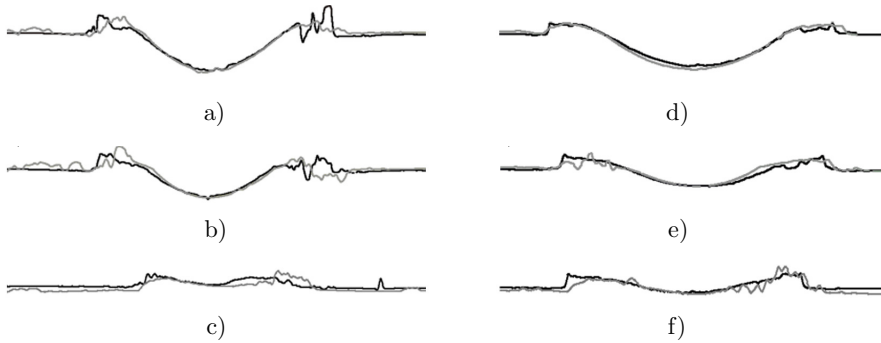

a)

d)

b)

e)

c)

f)

Fig. 20. Complete approximation of sample with 100 laser pulses engraved into steel in 2D view. Black curves represent cross-sections of the real sample and gray curves show the generated sample surface

seen in Figures 20 d)–f). The positions of the cross-sections in the sample are the same as in the previous example.

Figure 21 summarizes the 3D views on three different samples. The original samples with 10, 50, and 100 laser pulses engraved into steel are shown in the left column. They can be compared with the results of the sample approximation, which are placed in the right column. In the middle column, the situation after the first step of approximation (the smooth surface) is shown.

4 CONCLUSION, FUTURE PLANS

During our research we developed a number of methods, which can be used especially for real engraved and measured data preprocessing and description. All these methods were tested, compared and the best of them are incorporated into a tool for data preprocessing [11]. We decided to use such approach, because no fitting
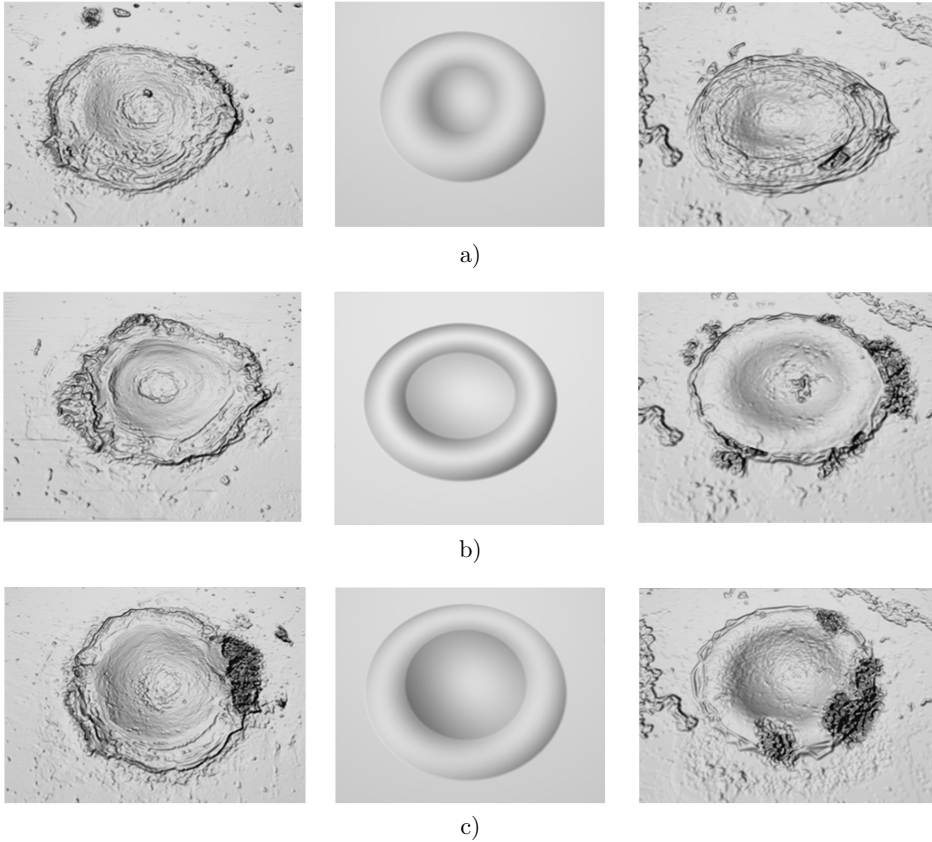
a)

b)

c)

Fig. 21. Real and generated samples: a) 10; b) 50; c) 100 laser pulses engraved into a single point in steel. In the left column the original samles are shown, in the middle column the smooth basic sample shapes can be seen and the sample approximation results are shown in the right column

methods were found before our data sets had to be processed. That is why we developed several methods for each individual data preprocessing step, we tested them and finally we selected methods with the best results. This paper describes our approaches with the best results and explains particular steps of data preprocessing. The whole research is described in detail in [9].

At this phase, we are able to explore samples in a very detailed way. The designed methods can be used for automatic detection of the heat-affected area. We are also able to describe the sample with a set of parameters and from their values; we can design a fully artificially generated new samples.

We have many plans for our future research, especially to work on modelling and simulation process and to improve it as much as we will be able to. Moreover,

we plan to maximize self-activity of the system by finding suitable methods for the sample parameterization (especially parameterization of sample roughness and irregularities) and other activities, which had to be done manually so far.

Acknowledgement

REFERENCES

[1] ACHARYA, T.—RAY, A. K.: Image Processing: Principles and Application. Wiley-Interscience 2005.

[2] ALEXIADES, V.—SOLOMON, A. D.: Mathematical Modelling of Melting and Freezing Processes. Taylor & Francis 1993.

[3] ANISIMOV, S. I.: Vaporization of Metal Absorbing Laser Radiation. Soviet Physics JETP, Vol. 27, 1968.

[4] BUERLE, D.: Laser Processing and Chemistry. Springer Verlag, Berlin 2000.

[5] DAHOTRE, N. B.—HARIMKAR, S. P.: Laser Fabrication and Machining of Materials. Springer, New York, USA 2008.

[6] HÁJKOVÁ, J.: Laser Simulation – Methods of Pulse Detection in Laser Simulation. In: Cordeiro, J., Shishkov, B., Ranchordas, A., Helfert, M. (Eds.): Proceedings of the 3rd International Conference on Software and Data Technologies ICSOFT 2008, INSTICC, Porto, Portugal 2008, pp. 186–191.

[7] HÁJKOVÁ, J.: Approaches for Automatic Comparison of Laser Burned Samples. Proceedings of the 9th International Ph. D. Workshop on Systems and Control, Izola, Slovenia 2008.

[8] HÁJKOVÁ, J.: Parameterization of Samples and Its Usage in Data Description and Simulation. In: Otamendi, J., Bargiela, A., Montes, J. L., Pedrera, L. M. D. (Eds.): Proceedings of the 23rd European Conference on Modeling and Simulation (ECMS 2009), Madrid, Spain 2009.

[9] HÁJKOVÁ, J.: Data Processing for Simulation of Laser Beam Impact. Doctoral Thesis, University of West Bohemia, Pilsen 2009.

[10] HARALICK, R. M.—SHAPIRO, G. L.: Computer and Robot Vision. Volume I. Addison-Wesley, Longman Publishing Co. Inc., Boston, MA, USA 1992.

[11] LASER BURNED SAMPLES EXPLORER. AVAILABLE ON: `http://www.kiv.zcu.cz/hajkovaj/sw/HeightMapViewer/`, 2012.

[12] PERLIN, K.: An Image Synthetizer. In: P. Cole, R. Heilman, B. A. Barsky (Eds.): Proceedings of the 12th Annual Conference on Computer Graphics and Interactive techniques, ACM New York, USA 1985, pp. 287–296.

[13] PERLIN, K.: Improving noise. In: T. Appolloni (Ed.): Proceedings of the 29th Annual Conference on Computer Graphics and Interactive Techniques, ACM New York, USA 2002, pp. 681–682.

[14] PERLIN NOISE. AVAILABLE ON: `http://freespace.virgin.net/hugo.elias/models/m_perlin.htm`, 2012.

[15] REKTORYS, K.: Přehled užité matematiky (A Survey of Applied Mathematics). SNTL Praha, Czech Republic 1981 (in Czech).

[16] SHAPIRO, L.—STOCKMAN, G.: Computer Vision. Prentice Hall, New Jersey, USA 2001.

[17] SONKA, M.—HLAVAC, V.—BOYLE, R.: Image Processing, Analysis, and Machine Vision, International Student Edition Nelson Engineering. Student Ed. Edition 2007.

[18] STEEN, W. M.: Laser Material Processing. Springer-Verlag, New York Berlin Heidelberg 1991.

[19] WEISSTEIN, E. W.: The CRC Concise Encyclopedia of Mathematics. CRC Press LLC, USA 1999.

[20] ŽÁRA, J.—BENEŠ, B.—FELKL P.: Moderní počítačová grafika (Modern Computer Graphics). Computer Press Brno, Czech Republic 2005 (in Czech).

Jana HÁJKOVÁ works as a lecturer at the University of West Bohemia. Her research interests include data visualization and computer simulation. She received her M. Sc. and Ph. D. degrees in computer science from the University of West Bohemia in 2005 and 2009, respectively.